HAL
open science

The effect of the north-east ice stream on the Greenland ice sheet in changing climates

R. Greve, S. Otsu

To cite this version:

R. Greve, S. Otsu. The effect of the north-east ice stream on the Greenland ice sheet in changing climates. The Cryosphere Discussions, 2007, 1 (1), pp.41-76. hal-00298522

HAL Id: hal-00298522

https://hal.science/hal-00298522v1

Submitted on 18 Jun 2008

HAL is a multi-disciplinary open access archive for the deposit and dissemination of scientific research documents, whether they are published or not. The documents may come from teaching and research institutions in France or abroad, or from public or private research centers.

L'archive ouverte pluridisciplinaire **HAL**, est destinée au dépôt et à la diffusion de documents scientifiques de niveau recherche, publiés ou non, émanant des établissements d'enseignement et de recherche français ou étrangers, des laboratoires publics ou privés.

The Cryosphere Discuss., 1, 41–76, 2007
www.the-cryosphere-discuss.net/1/41/2007/
© Author(s) 2007. This work is licensed
under a Creative Commons License.

The Cryosphere Discussions

The Cryosphere Discussions is the access reviewed discussion forum of *The Cryosphere*

The effect of the north-east ice stream on the Greenland ice sheet in changing climates

R. Greve[1] and S. Otsu[2,1]

[1]Institute of Low Temperature Science, Hokkaido University, Kita-19, Nishi-8, Kita-ku, Sapporo 060-0819, Japan
[2]Graduate School of Environmental Science, Hokkaido University, Kita-10, Nishi-5, Kita-ku, Sapporo 060-0810, Japan

Received: 1 June 2007 – Accepted: 8 June 2007 – Published: 20 June 2007

Correspondence to: R. Greve (greve@lowtem.hokudai.ac.jp)

Abstract

The north-east Greenland ice stream (NEGIS) was discovered as a large fast-flow feature of the Greenland ice sheet by synthetic aperture radar (SAR) imaginary of the ERS-1 satellite. In this study, the NEGIS is implemented in the dynamic/thermodynamic, large-scale ice-sheet model SICOPOLIS (Simulation Code for POLythermal Ice Sheets). In the first step, we simulate the evolution of the ice sheet on a 10-km grid for the period from 250 ka ago until today, driven by a climatology reconstructed from a combination of present-day observations and GCM results for the past. We assume that the NEGIS area is characterized by enhanced basal sliding compared to the "normal", slowly-flowing areas of the ice sheet, and find that the misfit between simulated and observed ice thicknesses and surface velocities is minimized for a sliding enhancement by the factor three. In the second step, the consequences of the NEGIS, and also of surface-meltwater-induced acceleration of basal sliding, for the possible decay of the Greenland ice sheet in future warming climates are investigated. It is demonstrated that the ice sheet is generally very susceptible to global warming on time-scales of centuries and that surface-meltwater-induced acceleration of basal sliding can speed up the decay significantly, whereas the NEGIS is not likely to dynamically destabilize the ice sheet as a whole.

1 Introduction

The Greenland ice sheet is the second-largest land ice mass on the present-day earth (Fig. 1). Its volume amounts to 2.85×10^6 km^3 or 7.2 m sea-level equivalent, the ice-covered area is 1.71×10^6 km^2, and the annual mass gain (accumulation rate) is 570 km^3 a^{-1} (Church et al., 2001). 50–60% of the total annual mass loss is due to surface melting and subsequent runoff into the sea, and the remainder is made up of calving (iceberg production) and a small amount of basal melting. The overall mass balance is probably slightly negative (Church et al., 2001; Thomas, 2004). Surface

melting will increase strongly with rising surface temperatures, which makes the ice sheet very susceptible to global warming.

The coastward mass flux of the ice sheet is drained by two major ice streams and a large number of outlet glaciers (Fig. 1). The Jakobshavn ice stream (JIS) in central west Greenland is a highly localized fast-flow feature, the speed of which has doubled since 1995 and reaches extremely large values of up to 13 km a^{-1} (Joughin et al., 2004). By contrast, the north-east Greenland ice stream (NEGIS), discovered first by Fahnestock et al. (1993) by means of synthetic aperture radar (SAR) imagery from the European Space Agency's ERS-1 satellite, is a large fast-flow feature with a length of ≈500 km and a maximum width of ≈100 km. The NEGIS branches into three major outlet glaciers close to the coast, where flow velocities of up to 1.2 km a^{-1} are reached (Joughin et al., 2001), an order of magnitude less than for the JIS.

This modelling study focuses on the effect of the NEGIS on the large-scale evolution and dynamics of the Greenland ice sheet. The ice-sheet model SICOPOLIS (SImulation COde for POLythermal Ice Sheets) is sketched in Sect. 2, and a paleoclimatic reference simulation without special consideration of the NEGIS is described in Sect. 3.1. The NEGIS is then implemented in SICOPOLIS by prescribing its areal extent based on data. Enhanced basal sliding in this area is quantified by seeking optimum agreement between simulated and observed ice thicknesses and surface velocities (Sect. 3.2). Using this calibration, global warming simulations are set up, which cover the period from 1990 CE until 2350 CE and are driven by the WRE scenarios (which assume a stabilization of the atmospheric CO_2 content on a higher level than today at some time in the future). In Sect. 4.1, the impact of enhanced basal sliding in the NEGIS area on ice-sheet decay is investigated, and, in addition, Sect. 4.2 deals with the possibility of surface-meltwater-induced speed-up of basal sliding in the entire ice sheet. Section 5 concludes the paper.

2 Modelling approach

The model SICOPOLIS simulates the large-scale dynamics and thermodynamics (extent, thickness, velocity, temperature, water content and age) of ice sheets three-dimensionally and as a function of time (Greve, 1997b). It is based on the shallow-ice approximation (Hutter, 1983; Morland, 1984) and the rheology of an incompressible, heat-conducting, power-law fluid (Glen's flow law, see Paterson, 1994). The thermo-mechanical coupling is described by the temperature- and water-content-dependent rate factor in the form of Greve et al. (1998) which follows Paterson's (1994) recommendations. A particular feature of the model thermodynamics is that it is distinguished between *cold ice* (with a temperature below the pressure melting point) and *temperate ice* (with a temperature at the pressure melting point) in a physically adequate fashion (Greve, 1997a). Isostatic depression and rebound of the lithosphere due to changing ice load is modelled by the local-lithosphere-relaxing-asthenosphere (LLRA) approach with an isostatic time lag τ_{iso} (Le Meur and Huybrechts, 1996; Greve, 2001).

External forcing is specified by (i) the mean annual air temperature at the ice surface, (ii) the surface mass balance (accumulation, ablation), (iii) the global sea level which defines the land area available for glaciation and (iv) the geothermal heat flux prescribed at the bottom of the lithospheric thermal boundary layer. All computations are carried out on a 10-km grid in the stereographic plane with standard parallel at 71°N and central meridian at 44°W, spanned by the Cartesian coordinates x and y. The vertical coordinate z is taken positive upward, and the zero level is the present-day reference geoid. The distortions due to the stereographic projection are corrected by appropriate metric coefficients. The model domain covers the entire area of Greenland and the surrounding sea. This leads to 165 by 281 grid points in the stereographic plane. In the vertical, σ coordinates are used, in that the cold-ice column, the temperate-ice layer (if present) and the lithosphere layer are mapped separately to [0, 1] intervals. The cold-ice column is then discretized by 81 grid points (which densify towards the base), and the temperate-ice and lithosphere layers are discretized each

by 11 equidistant grid points.

The standard values of the relevant physical parameters used for the simulations herein are listed in Table 1.

3 Paleoclimatic simulations

3.1 Reference simulation

Except for the doubled horizontal resolution (10 km instead of 20 km), the set-up of the reference simulation (run #1) is that of simulation hf_pmod2 described by Greve (2005). Model time is from 250 ka ago until today. The simulation is driven by a paleoclimatic forcing constructed by observed present-day climatologies (surface temperature, precipitation), their LGM (21 ka ago) counterparts from results of the PMIP UKMO general circulation model (Hewitt and Mitchell, 1997), and a weighed interpolation with a glacial index g. The latter is based on surface-temperature histories from the Greenlandic GRIP δ^{18}O record (Dansgaard et al., 1993; Johnsen et al., 1995) from today back until 105 ka ago, and from the Antarctic Vostok δD record (Petit et al., 1999) prior to 105 ka ago. It is scaled such that g=0 corresponds to the present-day interglacial climate, and g=1 denotes the LGM climate (Fig. 2). Surface melting is parameterized by Reeh's (1991) degree-day method, supplemented by explicit consideration of rainfall and the semi-analytical solution for the positive-degree-day integral by Calov and Greve (2005). Sea-level forcing is derived from the SPECMAP marine δ^{18}O record (Imbrie et al., 1984) converted to global sea level. For details see Greve (2005).

The spatially variable geothermal heat flux has been constructed by using the spherical-harmonic representation to degree and order 12 of the global heat flow by Pollack et al. (1993) as a background, determining optimum values of the heat flux at the four deep-ice-core locations GRIP, NGRIP, Camp Century and Dye 3 by matching simulated and observed basal temperatures, and interpolating an improved heat-flux distribution for the model domain. This was carried out by Greve (2005) for the 20-km

grid, and has been repeated here for the 10-km grid. This leads to the following set of values for the ice-core sites,

$$\begin{aligned} &\text{GRIP:} && q_{\text{geo}} = 59\,\text{mW}\,\text{m}^{-2}, \\ &\text{NGRIP:} && q_{\text{geo}} = 135\,\text{mW}\,\text{m}^{-2}, \\ &\text{Camp Century:} && q_{\text{geo}} = 54\,\text{mW}\,\text{m}^{-2}, \\ &\text{Dye 3:} && q_{\text{geo}} = 26\,\text{mW}\,\text{m}^{-2} \end{aligned} \tag{1}$$

(compared to 60, 135, 50 and 20 mW m^{-2}, respectively, for the 20-km grid). Figure 3 shows the resulting distribution of the geothermal heat flux.

Basal sliding is described by a Weertman-type sliding law in the form of Greve (2005), based on Greve et al. (1998) and modified to allow for sub-melt sliding (Hindmarsh and Le Meur, 2001),

$$v_{\text{b}} = -C_{\text{b}}\, e^{T'_{\text{b}}/\gamma_{\text{sms}}} \times \frac{\tau_{\text{b}}^{p}}{P_{\text{b}}^{q}}, \tag{2}$$

where v_{b} is the basal-sliding velocity, $C_{\text{b}}=C_{\text{b}}^{0}=11.2\,\text{m}\,\text{a}^{-1}\,\text{Pa}^{-1}$ the sliding coefficient, τ_{b} the basal shear traction in the bed plane, ρ the ice density, g the gravity acceleration, H the ice thickness and $P_{\text{b}}=\rho g H$ the overburden pressure. The stress and pressure exponents are chosen as $p=3$ and $q=2$. The term $e^{T'_{\text{b}}/\gamma_{\text{sms}}}$ represents the exponentially diminishing sub-melt sliding, where T'_{b} is the temperature relative to pressure melting (in °C) and $\gamma_{\text{sms}}=1$°C the sub-melt-sliding coefficient.

The simulated present-day surface topography is shown in Fig. 4 (left panel). The ice volume (3.141×10^{6} km^{3}) is 7.1% too large compared to the observed value of 2.932×10^{6} km^{3} (based on the 10-km discretization). Most of this difference originates from simulated ice cover in areas where there is no ice in reality, in particular in Peary Land north of 82° N, and along the eastern ice margin between 68° N and 74° N. Nevertheless, the overall agreement with the observed topography (Fig. 1, left panel) is very satisfactory.

A more detailed comparison is done by plotting the difference between the simulated and the observed ice thickness (Fig. 4, right panel). The above-mentioned discrepancies in Peary Land and along the eastern margin are clearly visible. In addition, a systematic sectorial misfit becomes evident, in that the simulated ice thicknesses are generally too thin in the north-west and south-east, whereas they are too thick in the north-east and south-west. It is difficult to assess the reasons for this behaviour in detail, but it is most likely due to a combination of inaccuracies of the surface mass balance, geothermal heat flux and lacking ice-stream dynamics. A strong indication for the latter point is the fact that the drainage areas of the JIS and NEGIS clearly correlate with over-predicted ice thicknesses.

For the NEGIS area, this is further illustrated by Fig. 5, which shows the scatter between simulated and observed ice thicknesses H and surface velocities v_s (Bamber et al., 2001; Joughin et al., 2001) for all N grid points in the NEGIS area. Also, the mean and root-mean-square (RMS) misfits, defined as

$$\mathrm{Mean}_H = \frac{\sum_{i,j} [H_{\mathrm{sim}}(i,j) - H_{\mathrm{obs}}(i,j)]}{N} \tag{3}$$

and

$$\mathrm{RMS}_H = \sqrt{\frac{\sum_{i,j} [H_{\mathrm{sim}}(i,j) - H_{\mathrm{obs}}(i,j)]^2}{N}} \tag{4}$$

(and analogous definitions for Mean_{v_s} and RMS_{v_s}) are given. As stated above, the simulated ice thicknesses are systematically too large (with some exceptions in the poorly resolved thin parts of the ice stream close to the margin), and in addition, the simulated surface velocities are generally too small. Both findings indicate consistently that fast ice flow in the NEGIS area is not properly accounted for in the simulation.

3.2 Basal sliding enhancement in the NEGIS area

In addition to the set-up of the reference simulation, we now consider a different sliding law with more rapid basal sliding for the NEGIS area. In order to do so, the location of the NEGIS has been identified by informations about its length and width given by Fahnestock et al. (1993), and by the map of balance velocities by Bamber et al. (2001), in which the NEGIS and its margins are well identifiable (Fig. 1). A mask file has been created which distinguishes the NEGIS grid points in the 10-km grid of SICOPOLIS.

Two different approaches for the NEGIS sliding law are employed. In the first approach, the sliding coefficient $C_b = C_b^0$ in the regular sliding law (2) is simply replaced by

$$C_b = C_b^0 \, m \tag{5}$$

in the NEGIS area, where m (≥ 1) is the sliding enhancement factor. For runs #2–5, we employ values of m=2, 3, 4 and 5, respectively. Also, in order to save come computing time, the model time is only from 127 ka ago until today, and the output of the reference simulation (run #1) for 127 ka ago is used as initial condition.

In the second approach for the NEGIS sliding law, we try a linear law, that is, the values of the exponents are changed to p=1 and q=0 for the NEGIS area. This law relates the basal sliding velocity linearly to the shear traction, which can be justified by assuming shear deformation of a linear-viscous sediment layer of constant thickness between ice and bedrock as the cause for rapid sliding (e.g. Greve et al., 2006). For the sliding coefficient of this linear law, we define a reference value of $C_b^0 = 10^{-3}\,\mathrm{m\,a^{-1}Pa^{-1}}$, and the sliding coefficient is again expressed as $C_b = C_b^0\, m$ (see Eq. 5). For runs #6–9, factors m=1, 1.5, 1.75 and 2, respectively, are used. Outside the NEGIS area, the non-linear sliding law with p=3, q=2 and $C_b = C_b^0 = 11.2\,\mathrm{m\,a^{-1}\,Pa^{-1}}$ is retained. Like for runs #2–5, the model time is from 127 ka ago until today, with initial conditions provided by run #1.

The mean and RMS misfits of the ice thickness and the surface velocity in the NEGIS area are summarized in Tables 2 and 3, and the respective best agreements are

marked. For runs #2–5 (non-linear sliding law), the picture is clear, in that all four misfit parameters decrease, go through a minimum and then increase (in terms of absolute values) with increasing sliding enhancement factor m. The minimum ice-thickness misfit occurs for m=2 (mean) and 3 (RMS), and the minimum surface-velocity misfit occurs for m=4 (mean) and 3 (RMS). Thus, the overall best agreement is reached for run #3 with m=3.

By contrast, for runs #6–9 (linear sliding law), the results are far less convincing. While from the mean misfits of the ice thickness and surface velocity and the RMS misfit of the surface velocity, one may choose run #8 (m=1.75) as a compromise, the RMS misfit of the ice thickness is even worse than that of the reference run #1 for all cases. The bad performance of the linear sliding law is further demonstrated by the scatter plots for run #3 (Fig. 6) and run #8 (Fig. 7), which show that the agreement for both the ice thickness and the surface velocity is far better for run #3 than for run #8. Also, by comparing the scatter plots of run #3 and run #1 (Fig. 5), the clear improvement indicated by the misfit parameters is evident.

So we conclude that the linear sliding law for the NEGIS area must be discarded. The simulation with the best overall agreement for both the ice thickness and the surface velocity in the NEGIS area is run #3, which features the non-linear sliding law with an enhancement factor m=3. In other words, basal sliding in the NEGIS area is three times more pronounced than elsewhere in the ice sheet.

Let us discuss the results of run #3 in some more detail. Figure 8 depicts the simulated surface topography (left panel) and the difference between the simulated and the observed ice thickness (right panel). Comparison with Fig. 4 shows again that the agreement for the NEGIS area has improved significantly, in that the ice thickness misfit is no longer systematically over-predicted, and the remaining misfits are distinctly smaller and balanced between positive and negative values. The ice volume of run #3 is 3.111×10^6 km^3, about 3.0×10^4 km^3 or 1% less than that of the reference run #1, and still 6.1% larger than the observed value. Evidently, the impact of enhanced basal sliding in the NEGIS area on the Greenland ice sheet as a whole is limited.

The simulated surface velocity (Fig. 9, left panel) reproduces nicely the "backbone" ridge of the Greenland ice sheet which connects Dye 3, GRIP, NGRIP and Camp Century, with a further branch from NGRIP northward to Peary Land. Also, the organization of the coastward mass flux into several drainage areas becomes evident, including an indication of fast-flowing ice in the region of the JIS. As for the NEGIS area, comparison with the observed velocities (Fig. 9, right panel) reveals that the simulated ice stream, while clearly identifiable, is less localized than the real one. This is a consequence of our simplified approach of describing the ice-stream dynamics by enhanced basal sliding within the shallow-ice approximation, and of the limited grid resolution of 10 km.

Figure 10 shows the basal temperature (relative to the pressure melting point) computed with run #3. The results are very similar to those reported by Greve (2005). The large geothermal heat fluxes around NGRIP and in the entire north-eastern sector of the ice sheet, including the NEGIS area, lead to widespread pressure-melting conditions at the ice base. Basal melting also prevails in western Greenland in a wide flowband upstream of the JIS where the heat fluxes are lower. Naturally, the anomaly of very low heat fluxes around Dye 3 entails low basal temperatures in the central part of south Greenland. Owing to the tuning of the geothermal-heat-flux distribution by Eq. (1), agreement between simulated and observed basal temperatures at the four deep-ice-core sites (GRIP, NGRIP, Camp Century, Dye 3) is very good.

4 Global warming simulations

Having the effect of the NEGIS on the recent Greenland ice sheet calibrated by the sliding coefficient (5) with a sliding enhancement factor m=3, we now investigate the fate of the ice sheet under future global-warming conditions. We use the "WRE scenarios" as model scenarios, in which it is assumed that the global mean temperature change results from stabilization of the atmospheric CO_2 concentration at 450, 550, 650, 750 and 1000 ppm, respectively (Cubasch et al., 2001). The corresponding temperature scenarios are shown in Fig. 11.

Church et al. (2001, Table 11.13) report that nine different AOGCM experiments following the IS92a scenario for the 21st century provided a temperature change over the Greenland ice sheet in the range of 1.3 . . . 3.1 times the global mean change, with an average ratio of approx. 2. The increase in precipitation over Greenland was 2.7 . . . 7.8%/°C with an average of approx. 5%/°C. Here, these average sensitivities are transferred to the simulations forced by the WRE scenarios. Consequently, the surface temperatures shown in Fig. 11 are amplified by a factor 2 and imposed as uniform increases over the ice sheet, and the precipitations are assumed to increase by 5% per degree of ice-sheet-surface-temperature change.

In the following, only the end-member scenarios WRE450 and WRE1000 will be considered, and the model time is from 1990 CE until 2350 CE.

4.1 Influence of basal sliding enhancement in the NEGIS area

Runs #10 and #11 use the output of the reference simulation (run #1) for the present as initial conditions, and are driven by the scenarios WRE450 and WRE1000, respectively. The NEGIS is not accounted for (sliding enhancement factor m=1). By contrast, for runs #12 (WRE450) and #13 (WRE1000), the sliding enhancement factor m=3 is employed in the NEGIS area, and consequently they start with the present state of run #3.

The evolutions of the ice volume which result from the four runs are displayed in Fig. 12 (left panel). In all cases, the volume decreases monotonically over time and does not stabilize within the modelled period. Therefore, the increased precipitation rates under warmer conditions are always outweighed by increased surface melting. The influence of enhanced basal sliding in the NEGIS area is limited to the volume offset of approximately 3.0×10^4 km^3 or 0.07 m s.l.e. (sea level equivalent) between the different initial conditions (run #1 vs. 3), which remains constant for runs #10 vs. 12 (WRE450) and increases only slightly to 3.5×10^4 km^3 or 0.08 m s.l.e. for runs #11 vs. 13 (WRE1000). This means that the enhanced basal sliding in the NEGIS area does not have the potential to dynamically destabilize the ice sheet. This becomes also clear

by inspection of Fig. 12 (right panel), which shows the freshwater discharge for the four runs. While the discharge increases strongly in all cases compared to the 1990 value of 590 $km^3 a^{-1}$ (0.019 Sv), the curves for runs #10 and 12 (WRE450) and those for runs #11 and 13 (WRE1000) fall virtually together.

4.2 Surface-meltwater-induced basal sliding speed-up

Recent observations of accelerated ice flow in west Greenland indicate that surface meltwater percolating to the base may play a crucial role in provoking a fast reaction of ice-sheet flow on increased surface temperatures (Zwally et al., 2002). Therefore, let us now consider the possibility of surface-meltwater-induced acceleration of basal sliding. Parizek and Alley (2004) parameterize this process by assuming that, at any given position, sliding speed-up is linearly related to the cumulative amount of surface meltwater produced upstream of this position. Here, we employ a slightly simpler approach, which relates the sliding speed-up to the *local* surface meltwater rate M. This is expressed by the sliding law (2) with the sliding coefficient

$$C_b = C_b^0 \, m \, (1 + \gamma M), \tag{6}$$

where γ is the surface meltwater coefficient. Like in Eq. (5), the sliding enhancement factor m expresses the more rapid basal sliding of the NEGIS. For all simulations of this subsection, m=3 is used in the NEGIS area and m=1 elsewhere, and the present state of run #3 is used as initial condition.

An estimation of the value of γ, based on observational data for one location in central west Greenland reported by Zwally et al. (2002), is given in Appendix A. This value, γ=0.1 a m^{-1}, is employed for runs #14 (WRE450) and #15 (WRE1000). In Appendix A it is also argued that the estimation is not necessarily representative for the entire ice sheet over longer time-scales. Therefore, we investigate the effect of a significantly stronger basal sliding speed-up. For runs #16 (WRE450) and #17 (WRE1000), γ is set to 1 a m^{-1}, and for runs #18 (WRE450) and #19 (WRE1000), γ=5 a m^{-1} is employed.

The resulting evolutions of the ice volume and the freshwater discharge are plotted in Fig. 13. The effect of surface-meltwater-induced acceleration of basal sliding with the estimated coefficient γ=0.1 a m^{-1} is rather small. By 2350, the ice volume of run #14 is 2.7×10^4 km^3 or 0.06 m s.l.e. less than that of run #12 (WRE450), and the ice volume of run #15 is 5.6×10^4 km^3 or 0.13 m s.l.e. less than that of run #13 (WRE1000). By contrast, the effect becomes much more pronounced for the more extreme scenarios of runs #16–19, for which the decay of the ice sheet speeds up strongly, and, correspondingly, the freshwater discharges increase significantly.

Finally, Fig. 14 shows the simulated surface topography by 2350 for the WRE1000 runs #13 (no surface-meltwater-induced acceleration of basal sliding) and #19 (extreme surface-meltwater-induced acceleration of basal sliding with γ=5 a m^{-1}). In case of run #13, the ice sheet has retreated further inland along almost its entire perimeter. Compared to 1990, the volume has decreased by 0.69×10^6 km^3 or 1.6 m s.l.e., and the freshwater flux has increased to 3.8×10^3 km^3 a^{-1} (0.12 Sv), which is 6.4 times the 1990 value. In case of run #19, the ice retreat is similar to that of run #13 north of 68° N, whereas further south the ice sheet has disappeared almost completely. This goes along with a larger volume decrease of 1.47×10^6 km^3 or 3.4 m s.l.e., and a larger freshwater flux of 5.7×10^3 km^3 a^{-1} (0.18 Sv, 9.6 times the 1990 value). Discharge rates of that magnitude may have the potential to affect the thermohaline circulation in the north Atlantic, and therefore feed back significantly on the global climate system.

Comparison of the simulated 2350 topographies (Fig. 14) for the NEGIS area reveals that the resulting surface depression is more pronounced in run #19 than in run #13, which is due to the combined effect of enhanced basal sliding (m=3) and surface-meltwater-induced acceleration of basal sliding (γ=5 a m^{-1}). However, it is also evident that even this combined effect does not seriously destabilize the ice sheet as a whole. In the scenario of run #19, the dynamically induced acceleration of ice-sheet decay is essentially active all around the perimeter of the ice sheet, and the existence of the NEGIS is not a crucial factor for this process.

5 Conclusions

The evolution, dynamics and thermodynamics of the Greenland ice sheet was simulated with the model SICOPOLIS, driven by paleoclimatic as well as future global-warming scenarios. The resulting surface topographies and velocities of the paleoclimatic runs were used to calibrate enhanced basal sliding in the area of the north-east Greenland ice stream (NEGIS) by minimizing the misfit to their observational counterparts. Best agreement was reached by preserving the non-linear, hard-rock-type basal sliding law which holds for the rest of the ice sheet, and using a sliding enhancement factor $m = 3$. Therefore, basal sliding in the NEGIS area is three times stronger than normal basal sliding in the ice sheet, and this leads to an approximately 1% reduction of the volume of the present-day ice sheet.

Simulations into the future showed clearly a strong susceptibility of the Greenland ice sheet to global warming on time-scales of centuries. However, the enhanced basal melting in the NEGIS area calibrated by the paleoclimatic simulations does not speed up the decay of the ice sheet significantly. By contrast, surface-meltwater-induced acceleration of basal sliding for the entire ice sheet can lead to a dynamic speed-up of its disintegration if the surface meltwater coefficient γ is an order of magnitude larger than the estimate of Appendix A. While this process was found to be enhanced moderately in the NEGIS area, the presence of the NEGIS is not crucial for it. So we finally conclude that the NEGIS, unless it behaves in an unexpected way by dramatically increasing its area or speeding up beyond our reasoning, can increase the decay of the Greenland ice sheet to a limited extent, but does not have the potential to dynamically destabilize the ice sheet as a whole.

Appendix A

Estimation of the surface-meltwater coefficient

If for a certain location on the ice sheet the basal temperature is at the pressure melting point (T'_b=0°C) and ice-stream sliding enhancement does not occur (m=1), the Weertman-type sliding law (2) with inserted values for the exponents p and q and the sliding coefficient (6) reads

$$v_b = C_b^0 (1 + \gamma M) \frac{\tau_b^3}{P_b^2} \tag{A1}$$

(signs not considered here). Thus, the part

$$\Delta v_b = C_b^0 \gamma M \frac{\tau_b^3}{P_b^2} \tag{A2}$$

can be attributed to meltwater-induced acceleration. If we employ the relations

$$P_b = \rho g H, \quad \tau_b = \rho g H |\nabla h| \tag{A3}$$

(where h denotes the ice surface elevation), this can be written as

$$\Delta v_b = C_b^0 \gamma M \rho g H |\nabla h|^3. \tag{A4}$$

The degree-day model yields for the melting rate

$$M = \max \left[\beta_{\text{ice}} \left(\frac{PDD}{\Delta t_m} - \frac{P_{\max} S}{\beta_{\text{snow}}} \right), 0 \right], \tag{A5}$$

where PDD are the positive-degree days during the melting season of duration Δt_m, S is the solid precipitation (snowfall) rate, and β_{ice}, β_{snow} and $P_{\max}$ are parameters.

In order to get a concrete estimate for the surface-meltwater coefficient γ, we use data from the Swiss Camp in central west Greenland. Zwally et al. (2002) report

for the summer of 1998 a value of PDD=116.5°C d for the summer melting season ($\Delta t_m \approx 120$ d). With the snowfall rate $S \approx 220$ mm w.e. a$^{-1} \approx 0.6$ mm w.e. d^{-1} (Ohmura and Reeh, 1991) and the parameters β_{ice}=7 mm w.e. d^{-1} °C^{-1}, β_{snow}=3 mm w.e. d^{-1} °C^{-1}, P_{max}=0.6, Eq. (A5) yields a melting rate of

$$M \approx 6\,\text{mm w.e. d}^{-1} \approx 6.5\,\text{mm i.e. d}^{-1}. \tag{A6}$$

The increase of ice-flow velocity during the summer of 1998 was 88 mm d^{-1} (Zwally et al., 2002). If we identify this increase with the meltwater-induced acceleration of basal sliding Δv_b, Eq. (A4) can be solved for the coefficient γ,

$$\gamma = \frac{\Delta v_b}{C_b^0 M \rho g H |\nabla h|^3}. \tag{A7}$$

With the ice thickness H=1220 m and the surface slope $|\nabla h| \approx 0.01$ (Parizek and Alley, 2004), Eq. (A7) yields a value for the surface-meltwater coefficient of

$$\gamma \approx 0.1\,\text{a m}^{-1}. \tag{A8}$$

However, note that this estimate holds only for one particular position and one particular year. Therefore, it is not necessarily representative for the entire ice sheet over longer time-scales, and a suitable overall value may differ from this estimate substantially.

Acknowledgements. This study is based on the master thesis by Otsu (2007). The authors wish to thank T. Hondoh and S. Sugiyama for co-supervising the thesis.

This research was supported by a Grant-in-Aid for Scientific Research (No. 18340135) from the Japan Society for the Promotion of Science.

Figure 1 (right panel) reproduced by permission of the American Geophysical Union.

References

Bamber, J. L., Layberry, R. L., and Gogenini, S. P.: A new ice thickness and bed data set for the Greenland ice sheet 1. Measurement, data reduction, and errors, J. Geophys. Res., 106, 33 773–33 780, 2001. 47, 48, 63

Calov, R. and Greve, R.: A semi-analytical solution for the positive degree-day model with stochastic temperature variations, J. Glaciol., 51, 173–175, 2005. 45

Church, J. A., Gregory, J. M., Huybrechts, P., Kuhn, M., Lambeck, K., Nhuan, M. T., Qin, D., and Woodworth, P. L.: Changes in sea level, in: Climate Change 2001: The Scientific Basis. Contribution of Working Group I to the Third Assessment Report of the Intergovernmental Panel on Climate Change, edited by Houghton, J. T., Ding, Y., Griggs, D. J., Noguer, M., van der Linden, P. J., Dai, X., Maskell, K., and Johnson, C. A., pp. 639–693, Cambridge University Press, Cambridge etc., 2001. 42, 50

Cubasch, U., Meehl, G. A., Boer, G. J., Stouffer, R. J., Dix, M., Noda, A., Senior, C. A., Raper, S., and Yap, K. S.: Projections of future climate change, in: Climate Change 2001: The Scientific Basis. Contribution of Working Group I to the Third Assessment Report of the Intergovernmental Panel on Climate Change, edited by Houghton, J. T., Ding, Y., Griggs, D. J., Noguer, M., van der Linden, P. J., Dai, X., Maskell, K., and Johnson, C. A., pp. 525–582, Cambridge University Press, Cambridge etc., 2001. 50, 73

Dansgaard, W., Johnsen, S. J., Clausen, H. B., Dahl-Jensen, D., Gundestrup, N. S., Hammer, C. U., Hvidberg, C. S., Steffensen, J. P., Sveinbjörnsdottir, A. E., Jouzel, J., and Bond, G.: Evidence for general instability of past climate from a 250-kyr ice-core record, Nature, 364, 218–220, 1993. 45

Fahnestock, M., Bindschadler, R., Kwok, R., and Jezek, K.: Greenland ice sheet surface properties and ice dynamics from ERS-1 SAR imagery, Science, 262, 1530–1534, 1993. 43, 48

Greve, R.: A continuum-mechanical formulation for shallow polythermal ice sheets, Phil. Trans. R. Soc. Lond., A355, 921–974, 1997a. 44

Greve, R.: Application of a polythermal three-dimensional ice sheet model to the Greenland ice sheet: Response to steady-state and transient climate scenarios, J. Climate, 10, 901–918, 1997b. 44

Greve, R.: Glacial isostasy: Models for the response of the Earth to varying ice loads, in: Continuum Mechanics and Applications in Geophysics and the Environment, edited by Straughan, B., Greve, R., Ehrentraut, H., and Wang, Y., pp. 307–325, Springer, Berlin etc., 2001. 44

Greve, R.: Relation of measured basal temperatures and the spatial distribution of the geothermal heat flux for the Greenland ice sheet, Ann. Glaciol., 42, 424–432, 2005. 45, 46, 50

Greve, R., Weis, M., and Hutter, K.: Palaeoclimatic evolution and present conditions of the

Greenland ice sheet in the vicinity of Summit: An approach by large-scale modelling, Paleoclimates, 2, 133–161, 1998. 44, 46
Greve, R., Takahama, R., and Calov, R.: Simulation of large-scale ice-sheet surges: The ISMIP HEINO experiments, Polar Meteorol. Glaciol., 20, 1–15, 2006. 48
Hewitt, C. D. and Mitchell, J. F. B.: Radiative forcing and response of a GCM to ice age boundary conditions: cloud feedback and climate sensitivity, Climate Dyn., 13, 821–834, 1997. 45
Hindmarsh, R. C. A. and Le Meur, E.: Dynamical processes involved in the retreat of marine ice sheets, J. Glaciol., 47, 271–282, 2001. 46
Hutter, K.: Theoretical Glaciology; Material Science of Ice and the Mechanics of Glaciers and Ice Sheets, D. Reidel Publishing Company, Dordrecht, The Netherlands, 1983. 44
Imbrie, J., Hays, J. D., Martinson, D. G., McIntyre, A., Mix, A. C., Morley, J. J., Pisias, N. G., Prell, W. L., and Shackleton, N. J.: The orbital theory of Pleistocene climate: Support from a revised chronology of the marine δ^{18}O record, in: Milankovitch and Climate, Part I, edited by Berger, A., Imbrie, J., Hays, J., Kukla, G., and Saltzman, B., pp. 269–305, Reidel, Dordrecht, NATO ASI Series C: Mathematical and Physical Sciences 126, 1984. 45
Johnsen, S. J., Dahl-Jensen, D., Dansgaard, W., and Gundestrup, N.: Greenland palaeotemperatures derived from GRIP borehole temperature and ice core isotope profiles, Tellus, 47B, 624–629, 1995. 45
Joughin, I., Fahnestock, M., MacAyeal, D. R., Bamber, J. L., and Gogenini, S. P.: Observation and analysis of ice flow in the largest Greenland ice stream, J. Geophys. Res., 106, 34 021–34 034, 2001. 43, 47, 71
Joughin, I., Abdalati, W., and Fahnestock, M.: Large fluctuations in speed on Greenland's Jakobshavn Isbrae glacier, Nature, 432, 608–610, doi:10.1038/nature03130, 2004. 43
Le Meur, E. and Huybrechts, P.: A comparison of different ways of dealing with isostasy: examples from modelling the Antarctic ice sheet during the last glacial cycle, Ann. Glaciol., 23, 309–317, 1996. 44
Morland, L. W.: Thermo-mechanical balances of ice sheet flows, Geophys. Astrophys. Fluid Dyn., 29, 237–266, 1984. 44
Ohmura, A. and Reeh, N.: New precipitation and accumulation maps for Greenland, J. Glaciol., 37, 140–148, 1991. 56
Otsu, S.: The effect of the North-East Greenland Ice Stream (NEGIS) on the Greenland ice sheet in changing climates, Master thesis, Graduate School of Environmental Science, Hokkaido University, Sapporo, Japan, 2007. 56

Parizek, B. R. and Alley, R. B.: Implications of increased Greenland surface melt under global-warming scenarios: ice-sheet simulations, Quaternary Sci. Rev., 23, 1013–1027, doi:10.1016/j.quascirev.2003.12.024, 2004. 52, 56

Paterson, W. S. B.: The Physics of Glaciers, Pergamon Press, Oxford etc., 3rd edn., 1994. 44

Petit, J. R., Jouzel, J., Raynaud, D., Barkov, N. I., Barnola, J. M., Basile, I., Bender, M., Chappellaz, J., Davis, M., Delaygue, G., Delmotte, M., Kotlyakov, V. M., Legrand, M., Lipenkov, V. Y., Lorius, C., Pepin, L., Ritz, C., Saltzman, E., and Stievenard, M.: Climate and atmospheric history of the past 420 000 years from the Vostok ice core, Antarctica, Nature, 399, 429–436, 1999. 45

Pollack, H. N., Hurter, S. J., and Johnson, J. R.: Heat-flow from the Earth's interior: Analysis of the global data set, Rev. Geophys., 31, 267–280, 1993. 45, 65

Reeh, N.: Parameterization of melt rate and surface temperature on the Greenland ice sheet, Polarforsch., 59, 113–128, 1991. 45

Thomas, R. H.: Greenland: recent mass balance observations, in: Mass Balance of the Cryosphere. Observations and Modelling of Contemporary and Future Changes, edited by Bamber, J. L. and Payne, A. J., pp. 393–436, Cambridge University Press, Cambridge etc., 2004. 42

Zwally, H. J., Abdalati, W., Herring, T., Larson, K., Saba, J., and Steffen, K.: Surface melt-induced acceleration of Greenland ice-sheet flow, Science, 297, 218–222, 2002. 52, 55, 56

Table 1. Standard physical parameters of the ice-sheet model SICOPOLIS.
*: $E=1$ for Holocene or Eemian ice (deposited between 11 ka ago and the present, or between 132 and 114.5 ka ago), $E=3$ for Weichselian or pre-Eemian ice (deposited during other times).

Quantity	Value
Gravity acceleration, g	$9.81\,\mathrm{m\,s^{-2}}$
Density of ice, ρ	$910\,\mathrm{kg\,m^{-3}}$
Power-law exponent, n	3
Flow-enhancement factor, E	1 / 3*
Melting point at atmospheric pressure, T_0	273.15 K
Heat conductivity of ice, κ	$9.828\,e^{-0.0057\,T[\mathrm{K}]}\,\mathrm{W\,m^{-1}K^{-1}}$
Specific heat of ice, c	$(146.3 + 7.253\,T[\mathrm{K}])\,\mathrm{J\,kg^{-1}K^{-1}}$
Latent heat of ice, L	$335\,\mathrm{kJ\,kg^{-1}}$
Clausius-Clapeyron gradient, β	$8.7 \times 10^{-4}\,\mathrm{K\,m^{-1}}$
Density × specific heat of the lithosphere, $\rho_r c_r$	$2000\,\mathrm{kJ\,m^{-3}K^{-1}}$
Heat conductivity of the lithosphere, κ_r	$3\,\mathrm{W\,m^{-1}K^{-1}}$
Isostatic time lag, τ_{iso}	3000 a
Asthenosphere density, ρ_a	$3300\,\mathrm{kg\,m^{-3}}$

Table 2. Thickness and velocity misfits for runs #2–5 (non-linear sliding law in the NEGIS area, increasing sliding enhancement factor m) and the reference simulation (run #1). Smallest misfits are marked by boxes.

Run ($m \nearrow$)	Thickness (NEGIS) Mean of misfit [m]	Thickness (NEGIS) RMS of misfit [m]	Velocity (NEGIS) Mean of misfit [m a^{-1}]	Velocity (NEGIS) RMS of misfit [m a^{-1}]
#2	$\boxed{12.20}$	139.2	−24.74	71.23
#3	−37.80	$\boxed{137.1}$	−13.05	$\boxed{66.52}$
#4	−80.63	153.2	$\boxed{-0.88}$	68.72
#5	−116.6	173.5	9.35	72.32
#1	75.33	162.9	−38.54	78.68

Table 3. Thickness and velocity misfits for runs #6–9 (linear sliding law in the NEGIS area, increasing sliding enhancement factor m) and the reference simulation (run #1). Smallest misfits are marked by boxes.

Run ($m \nearrow$)	Thickness (NEGIS) Mean of misfit [m]	Thickness (NEGIS) RMS of misfit [m]	Velocity (NEGIS) Mean of misfit [m a^{-1}]	Velocity (NEGIS) RMS of misfit [m a^{-1}]
#6	99.56	190.1	−18.36	76.43
#7	48.42	180.4	$\boxed{0.52}$	71.00
#8	23.73	180.4	9.97	$\boxed{70.64}$
#9	$\boxed{-1.33}$	186.1	18.86	71.37
#1	75.33	$\boxed{162.9}$	−38.54	78.68

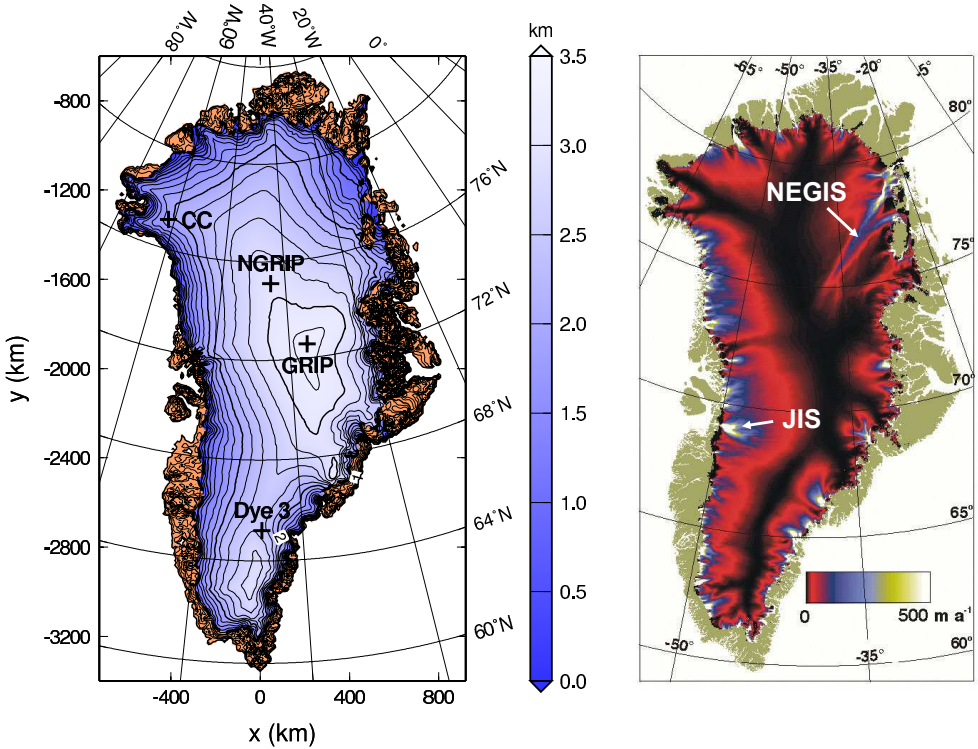

Fig. 1. Present-day Greenland ice sheet. Left panel: Observed surface topography (data by Bamber et al., 2001). Labels in km a.s.l., contour spacing 200 m. "Icy" hues indicate glaciated land, whereas brown areas are ice-free. Right panel: Balance velocities (plot by Bamber et al., 2001). The north-east Greenland ice stream (NEGIS) and the Jakobshavn ice stream (JIS) are clearly visible.

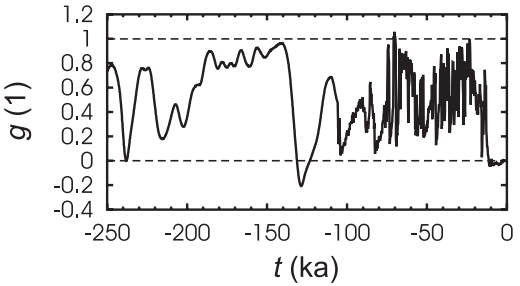

Fig. 2. Glacial index g, based on surface-temperature histories from the Greenlandic GRIP δ^{18}O record from today back until 105 ka ago, and from the Antarctic Vostok δD record prior to 105 ka ago.

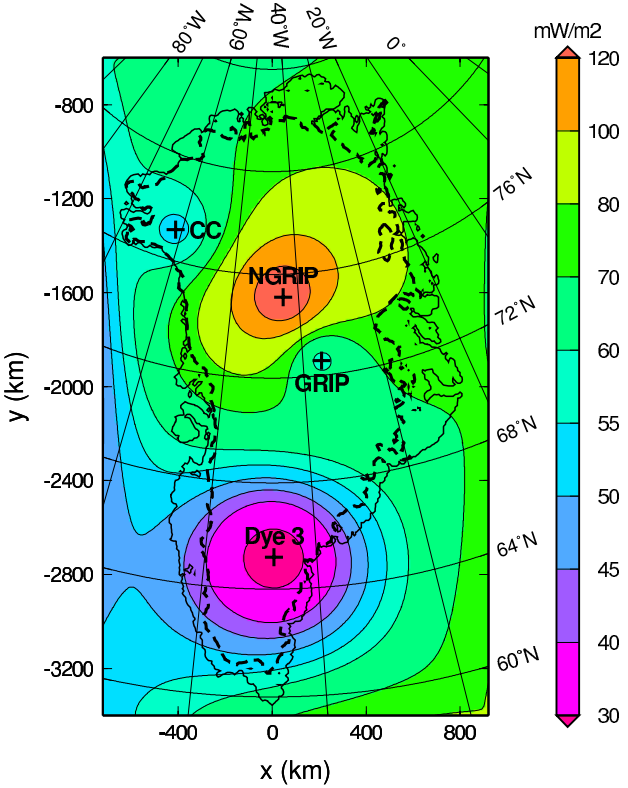

Fig. 3. Distribution of the geothermal heat flux based on Pollack et al. (1993) and the values of Eq. (1) for the ice-core sites GRIP, NGRIP, Camp Century and Dye 3. The heavy dashed line indicates the present-day ice margin.

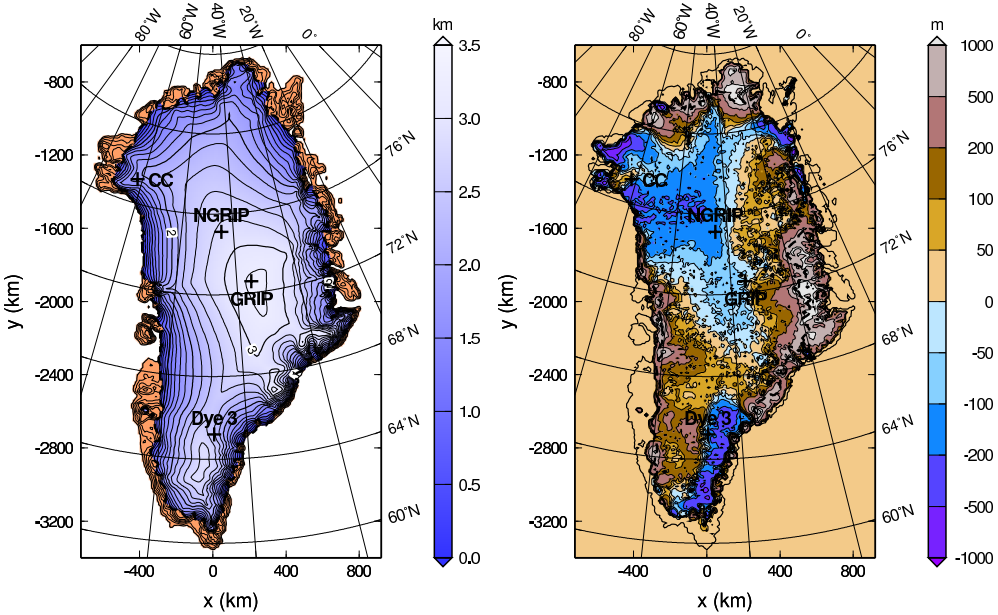

Fig. 4. Reference simulation (run #1): Present-day surface topography (left panel; contour spacing 200 m, labels in km a.s.l.), and difference between simulated and observed present-day ice thickness (right panel). The heavy dashed lines indicate the simulated (left panel) and observed (right panel) ice margins.

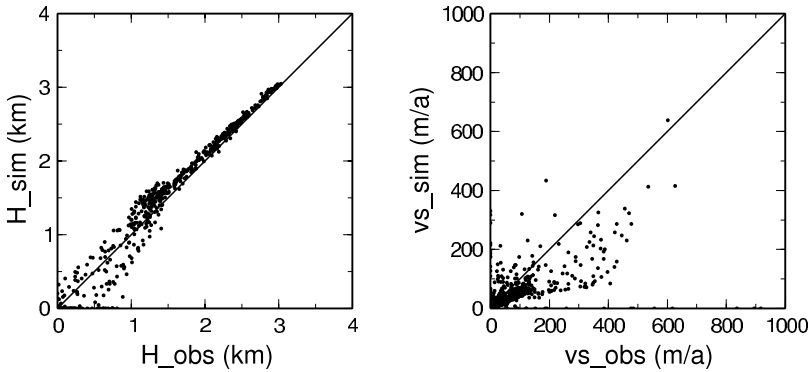

Mean of misfit: $+75.33\,\mathrm{m}$.
RMS of misfit: $162.9\,\mathrm{m}$.

Mean of misfit: $-38.54\,\mathrm{m\,a^{-1}}$.
RMS of misfit: $78.68\,\mathrm{m\,a^{-1}}$.

Fig. 5. Simulated vs. observed ice thicknesses H (left) and surface velocities v_s (right) in the NEGIS area for the reference simulation (run #1). Each dot represents one grid point.

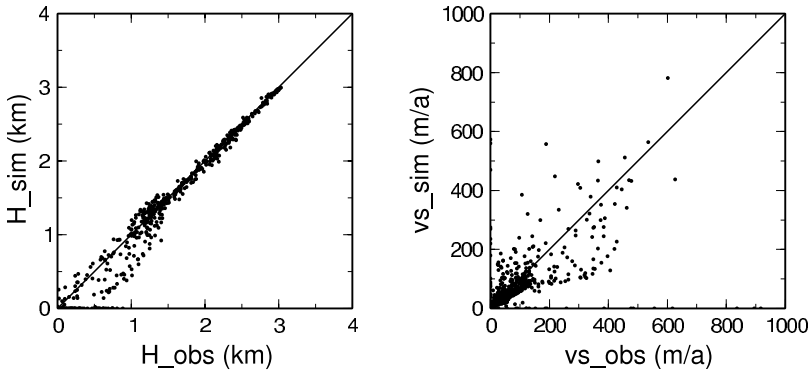

Mean of misfit: $-37.80\,\mathrm{m}$.
RMS of misfit: $137.1\,\mathrm{m}$.

Mean of misfit: $-13.05\,\mathrm{m\,a^{-1}}$.
RMS of misfit: $66.52\,\mathrm{m\,a^{-1}}$.

Fig. 6. Simulated vs. observed ice thicknesses H (left) and surface velocities v_s (right) in the NEGIS area for run #3. Each dot represents one grid point.

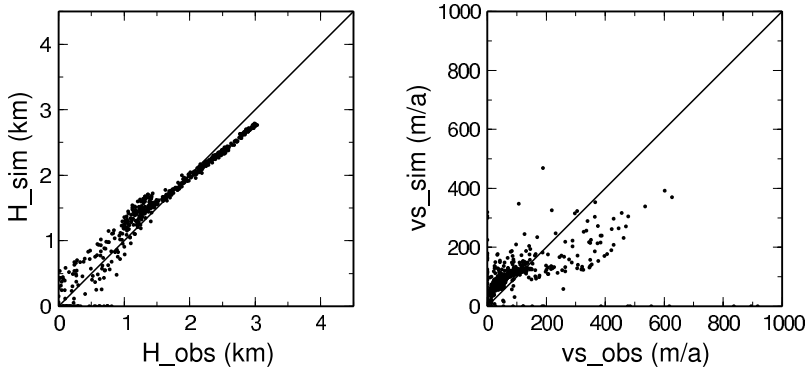

Mean of misfit: $+23.73\,\mathrm{m}$.
RMS of misfit: $180.4\,\mathrm{m}$.

Mean of misfit: $+9.97\,\mathrm{m\,a^{-1}}$.
RMS of misfit: $70.64\,\mathrm{m\,a^{-1}}$.

Fig. 7. Simulated vs. observed ice thicknesses H (left) and surface velocities v_s (right) in the NEGIS area for run #8. Each dot represents one grid point.

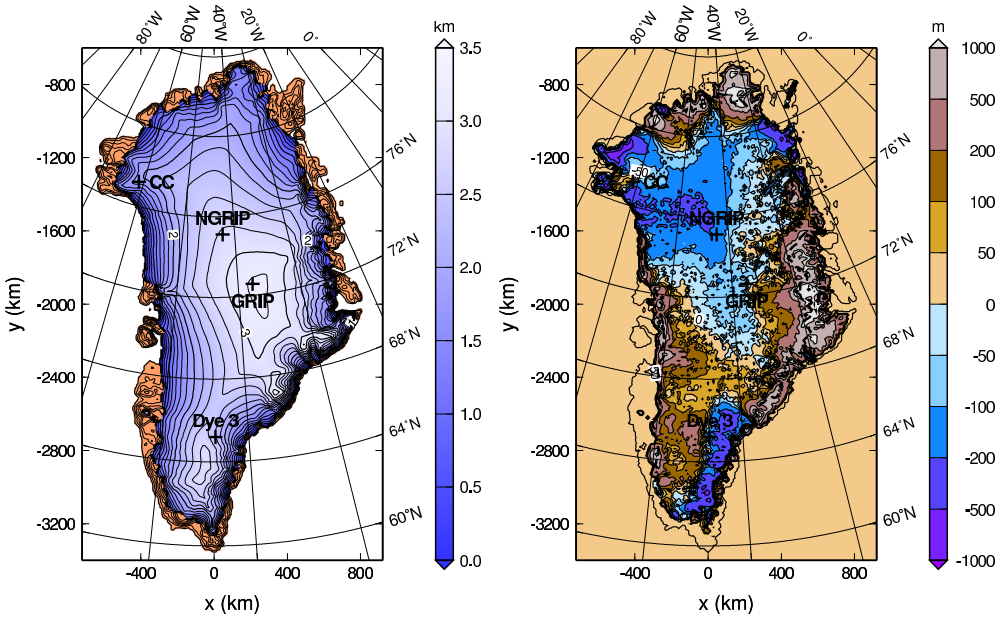

Fig. 8. Best-agreement simulation (run #3): Present-day surface topography (left panel; contour spacing 200 m, labels in km a.s.l.), and difference between simulated and observed present-day ice thickness (right panel). The heavy dashed lines indicate the simulated (left panel) and observed (right panel) ice margins.

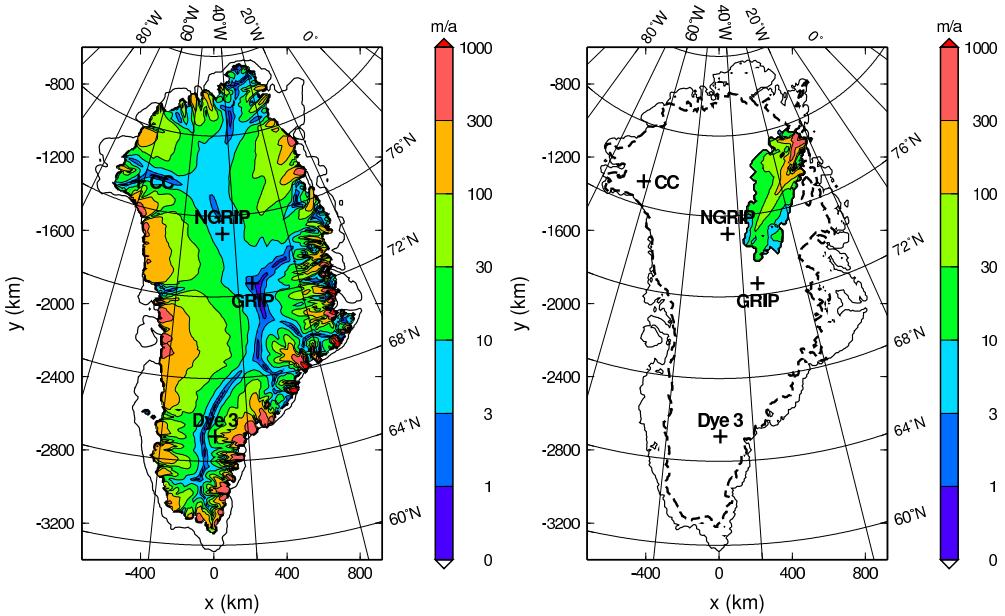

Fig. 9. Simulated (left panel; best-agreement run #3) vs. observed (right panel; Joughin et al., 2001; NEGIS area only) present-day surface velocities.

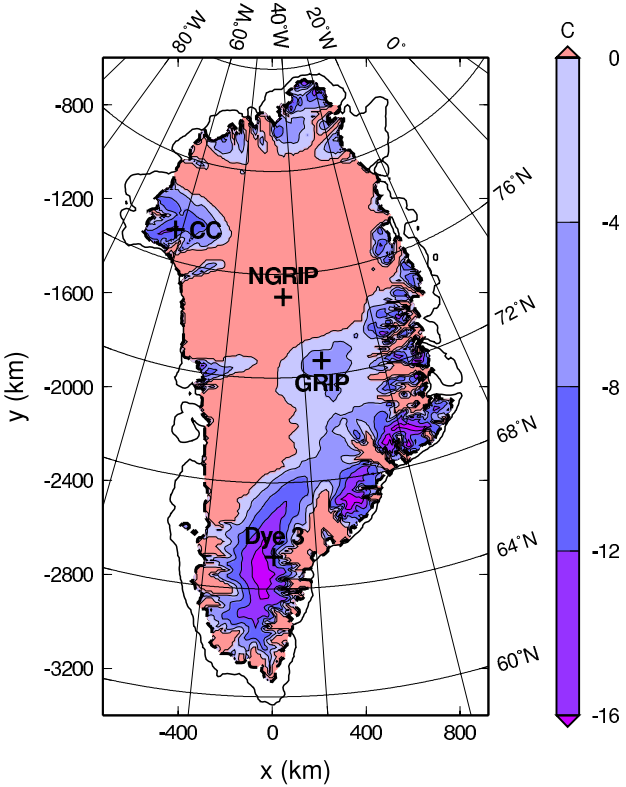

Fig. 10. Best-agreement simulation (run #3): Present-day basal temperature (relative to the pressure melting point). Red areas are at the pressure melting point.

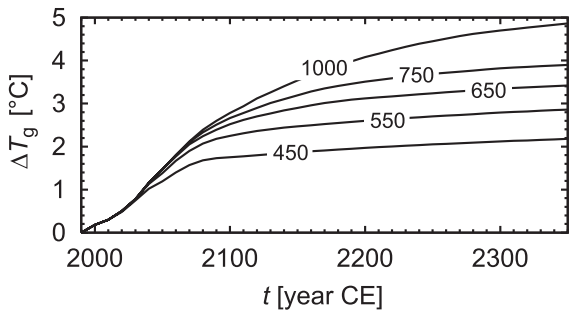

Fig. 11. Global mean temperature change ΔT_g for the profiles WRE450, WRE550, WRE650, WRE750 and WRE1000 (stabilization scenarios for atmospheric CO_2), by Cubasch et al. (2001).

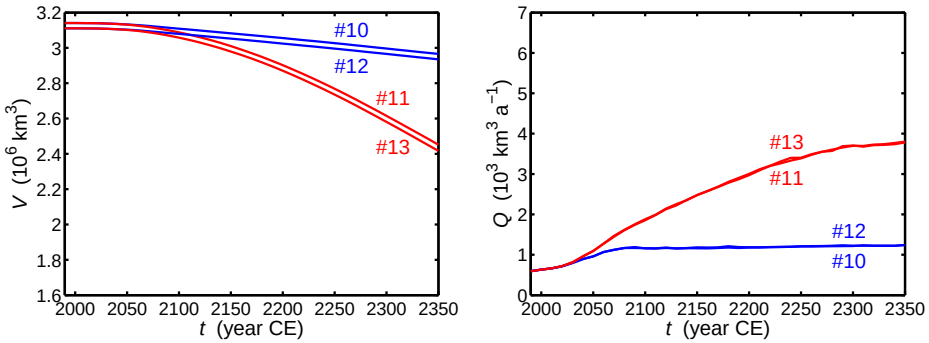

Fig. 12. Simulated evolution of the ice volume V and the freshwater discharge Q for the global warming runs #10 (no NEGIS, WRE450), #11 (no NEGIS, WRE1000), #12 (NEGIS / m=3, WRE450) and #13 (NEGIS / m=3, WRE1000). Note that blue and red curves correspond to the WRE450 and WRE1000 scenarios, respectively.

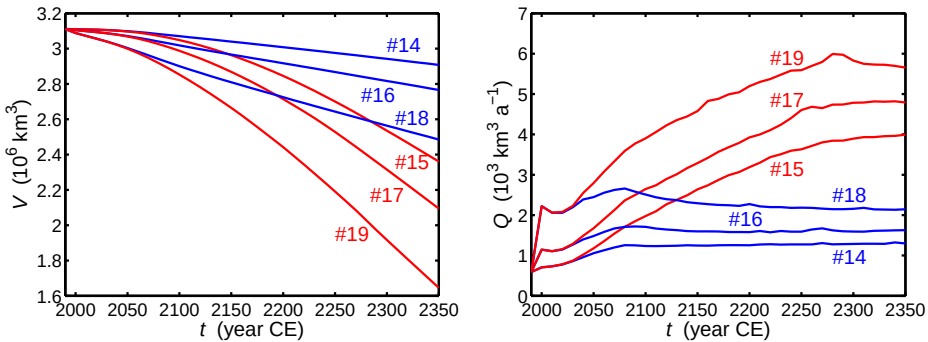

Fig. 13. Simulated evolution of the ice volume V and the freshwater discharge Q for the global warming runs #14 (NEGIS / m=3, WRE450, γ=0.1 a m^{-1}), #15 (NEGIS / m=3, WRE1000, γ=0.1 a m^{-1}), #16 (NEGIS / m=3, WRE450, γ=1 a m^{-1}), #17 (NEGIS / m=3, WRE1000, γ=1 a m^{-1}), #18 (NEGIS / m=3, WRE450, γ=5 a m^{-1}) and #19 (NEGIS / m=3, WRE1000, γ=5 a m^{-1}). Note that blue and red curves correspond to the WRE450 and WRE1000 scenarios, respectively.

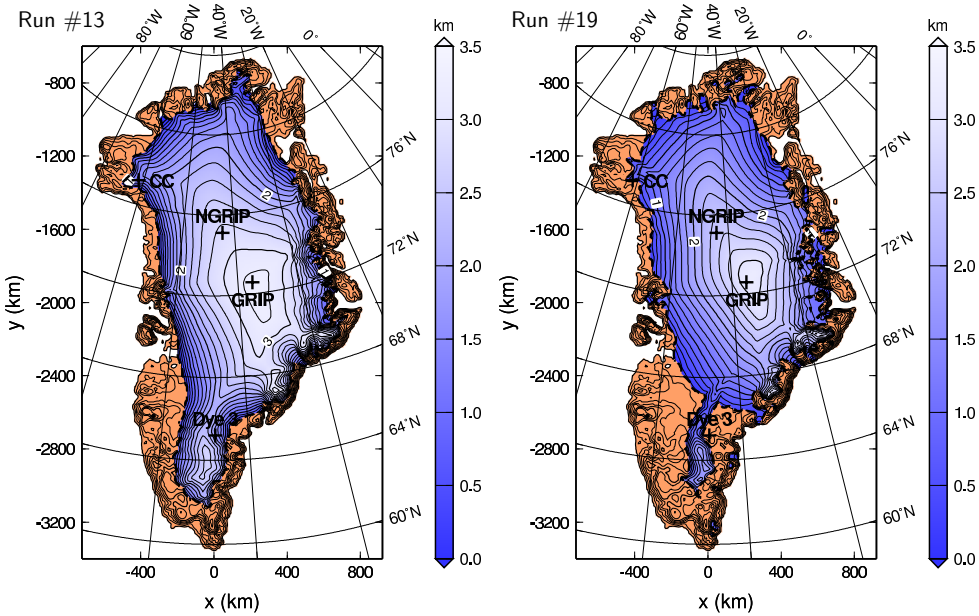

Fig. 14. Global warming runs #13 (NEGIS / m=3, WRE1000) and #19 (NEGIS / m=3, WRE1000, γ=5 a m^{-1}): Surface topography in 2350 CE. Contour spacing 200 m, labels in km a.s.l.